ELSEVIER

Journal of Physics and Chemistry of Solids 65 (2004) 1517–1526

JOURNAL OF PHYSICS AND CHEMISTRY OF SOLIDS

www.elsevier.com/locate/jpcs

α–β Inversion in quartz from low frequency electrical impedance spectroscopy

N.S. Bagdassarov*, N. Delépine

Institut für Meteorologie und Geophysik, Johann Wolfgang Goethe Universität-Frankfurt, Feldbergstraße 47, 60323 Frankfurt am Main, Germany

Received 23 June 2003; revised 15 October 2003; accepted 25 October 2003

Abstract

The α–β phase transformation in quartz has been studied in the pressure range from 0.5 to 2.5 GPa by the use of the low frequency electrical impedance spectroscopy. The electrical conductivity data obtained at low frequencies exhibit a different slope on an Arrhenius plot $\ln(\sigma^*_{LFD}T)$ vs. $1/T$ above and below T_c, where T is the absolute and T_c is the inversion temperature. The point where the slope changes, coincide with the T_c, i.e. the temperature point of α–β inversion in quartz. The obtained inversion temperature T_c from this method compares well with the previous measurements of T_c using DTA and laser interferometry. The low frequency dispersion data in insulating materials with the ionic conductivity due to impurities may be a useful method for characterization of structural displacive phase transitions in quartz-like structures.

Keywords: D. Phase transition

1. Introduction

The purpose of this study is to demonstrate the possibility of the impedance spectroscopy for study the structural phase transition in SiO_2 and to characterize well-known phase boundary of α–β inversion on SiO_2 phase diagram by using the low frequency dispersion (LFD) data of complex electrical impedance.

The α–β phase transition from trigonal to hexagonal high temperature symmetry is fully described in the literature [1,2]. Low temperature α-phase has a $P3_221$ ($P3_121$) space group, the high temperature β-phase represents $P6_422$ ($P6_222$) space group. The transition characterizes of the sudden increase of the thermal expansion coefficient, disappearance of the piezoelectric effect for the AT cut when the Si–O–Si angle equals 153° [3], anomalous behavior of the specific heat capacity, Raman mode softening at 207 cm^{-1} [4], frequencies of a number of longitudinal and transverse optical modes critically soften or harden in the α-phase in the vicinity of $T_c = 846$ K [5]. This transition is also characterized by the enhancement of the second harmonic generation of light [6] and the existence of a critical opalescence [7]. The transition from α to β phase is a displacive phase transition of the first-order with a symmetry breaking order parameter which can be described in a frame of Landau theory [8,9], but in the small temperature range 1.4 K just above the transition on cooling an incommensurate phase appears. The existence of this phase is caused by a coupling between soft mode and a transverse acoustic mode of phonons [1].

The quartz is an excellent insulating material because of the wide energy gap between valence state and Fermi level ~9 eV. The quartz conductivity and the activation energy of electrical conductivity are weak below 200 °C. At higher temperature the conductivity has strong features of the ionic type. SiO_2 represents highly ionic crystal and its chemical bonding is partially covalent [10]. Vacancies of oxygen are playing a minor role in the electrical transport in crystalline SiO_2 because of the large energy of formation, 6.79 eV for the neutral state of the vacancy [11]. The mechanism of electrical transport in quartz is influenced by the presence of $(Al^{3+}–M^{+})$-centers, substituting for Si^{4+} and ionic impurities M^+ like Li, Na, K or H [12]. The alkali ion is bounded with AlO_4^- by electrostatic attraction force and forms a Al–M pair, protons form a OH– bond near

* Corresponding author. Tel.: +49-69-798-23376; fax: +49-69-798-23280.

E-mail address: nickbagd@geophysik.uni-frankfurt.de (N.S. Bagdassarov).

0022-3697/$ - see front matter © 2004 Elsevier Ltd. All rights reserved.
doi:10.1016/j.jpcs.2003.10.075

Al-centers, Al^{3+} with non-compensated electrical charge forms $Al-h^+$ pair, where h^+ is a hole [13]. The bulk electrical conductivity in quartz structures is highly anisotropic, it is much higher along open channels parallel to the z-optical axis. The open channels in the structure of α and β-quartz favor the transport of ions. The dielectric constant anisotropy $\delta\varepsilon = \varepsilon_{11} - \varepsilon_{33} \approx 0.12$ in α-quartz [3]. With the pressure increase up to 5 GPa the decrease in anisotropy of the dielectric constant is expected $< 10\%$ ($\delta\varepsilon \approx 0.11$). The difference in the bulk electrical conductivity between α and β phase is negligible, the cross-section of channels along the z-axis at T_c drops insignificantly for about 3.4% and, thus, the electrical impedance cannot be used for the characterization of this phase transition. In contrast, the transition between β-phase and trydimite at 867 °C and atmospheric pressure has been identified once by the electrical conductivity measurements [14]. But this transformation is very sluggish in order to be properly characterized during heating–cooling cycles, by heating pure quartz bypasses tridymite and transforms directly into cristobalite at ~1050 °C [2].

At low frequencies the transport of charged species may be realized also along twin [15] and grain boundaries. Twin walls and antiphase boundaries can be enriched by ionic impurities and Al–M or Al–OH pairs. The overall effect of twin boundary presence in quartz may result in trapping and slower diffusion of along the z-axis and in enhanced electrical transport perpendicular to the z-axis. The effect of the twin boundary conductivity on the overall bulk conductivity is proportional to the ratio $\sim (d/L)\delta\sigma$, where d is a twin boundary thickness, L is the twin boundary length, $\delta\sigma$ is the excess of twin boundary conductivity over bulk conductivity in a twin domain interior [16]. Assuming that in polycrystalline samples $d/L \ll 1$, the effect of twin boundaries in the bulk properties will be negligible. In polycrystalline sample the conductivity also arises from enhanced mobility of ionic impurities along grain boundaries. The presence of twin and grain boundaries adjacent to electrodes probably would enhance the electrode polarization effect at low frequencies. Thus, during the α–β quartz transformation the difference in the resulted electrode polarization effect, consisting of the dipolar polarization of twin and grain boundaries and the charge-carrier polarization, may be measurable by doing the low frequency electrical impedance spectroscopy. In this experimental work the α–β inversion temperature has been estimated from low frequency electrical impedance measurements in compacted crystalline powder samples of SiO_2 at pressures from 0.5 to 2.5 GPa.

2. Experiments

2.1. Quartz samples

The high pressure experiments on natural polycrystalline compressed SiO_2 powder were done in the piston-cylinder apparatus. Powder samples with a grain size 20–30 were prepared from a piece of a natural quartz crystal Mont-Rose sampled from the outcrop of the French side of Grand Paradis (altitude about 2650 m, Bonneval-sur-Arc, France). Pieces of quartz crystals were selected under the microscope having no fluid and mineral inclusions. After grinding the powder was immersed in HCl to remove carbonates, washed in distilled water and dried (F. Brunet, personal communication). Typical concentrations of impurities in natural quartz crystals are 200–1200 ppm for H^+, 200–2000 for Li^+, 100–300 for Na^+, 1000–4000 for Al^{3+} [17]. Alkaline ions are sixfold coordinated interstitials with effective sizes 0.74 of Li^+ and 1.02 for Na^+, H^+ presenting as a diffusing fourfold coordinated OH^- on O sites behave as it is an interstitial with an anion size 1.52. Al^{3+} may be sixfold coordinated interstitial in z-channels or fourfold coordinated substitutional on other faces having the effective size 0.53 and 0.39, respectively [17].

2.2. Piston-cylinder

In this study a conventional piston-cylinder apparatus was used with a pressure cell consisting of CaF_2 and boron nitride as a confining medium and a graphite sleeve as a heater [18]. The experiments have been done at pressures from 0.5 up to 2.5 GPa and temperatures up to 1200 °C. The pressure calibration of the cell has been done by the use of some standard point materials: at room temperature the transformations Bi I–II–III at 2.56 and 2.7 GPa have been used; at high pressure the melting curves of NaCl and CsCl have been exploited. The melting points of these salts as a function of pressure up to 2.5 GPa has been determined in situ by electrical conductivity measurements. The performed pressure calibration is within an accuracy of ±30 MPa. The temperature gradient in the cell has been estimated on dummy samples of pressed Al_2O_3 powder by the use of three thermocouples. The estimation for a radial temperature gradient is ca. 1°/mm, for a vertical temperature gradient is ca. 2°/mm in the temperature range up to 900 °C. The constant pressure was provided by a servomotor which regulated a position of the piston in a separated hydraulic cylinder. The oil pressure in loading hydraulic rams was maintained within 0.05 MPa. Movement of the compressing piston in the autoclave was monitored with a position gauge having precision −0.001 mm.

2.3. Impedance spectroscopy

Electrical impedance measurements have been performed with the use of the Solartron® 1260 Phase-Gain-Analyzer interfaced with a PC. The device permits a single sine drive and analysis of a system under test over the frequency range 10 Hz to 32 MHz. In high pressure experiments 1 V sine signal was applied in frequency range 0.03 Hz to 300 kHz. A cell for electrical impedance measurements represents a coaxial cylindrical capacitor with a geometric factor 5–7 cm filled with a sample under

test. The exact geometric factor of a cell has been evaluated independently from calibration measurements on NaCl solutions (0.01–3 M) at 22 °C and pressure 0.1 MPa. For these purposes a cylindrical gap between two Pt-electrodes (made of Pt-tubes 0.1 mm in thickness) has been filled with a NaCl-solution of a known molar concentration. The measured conductivity of NaCl-solutions has been compared with the table values. The difference between a calculated geometric factor of the cylindrical capacitor and a measured geometric factor by using standard solutions was about 25%. The main advantage of the use of a coaxial cylinder geometry before a parallel plate geometry is a negligible change of the geometric factor under loading the sample [18].

During impedance measurements the press was separated from the ground of the Solartron 1260. One wires of Pt-thermocouple and the mass of the high pressure autoclave were used to connect the measuring device and the cell electrodes. Before doing the high pressure experiments, a measuring cell has been calibrated for a short circuit and for an open circuit impedances in a frequency range 1 MHz–0.01 Hz. A typical AC-resistance of the cell to a short circuit is 0.4 Ω. These calibrations have been taken into account in final calculations of the electrical impedance as a function of frequency. At high pressure and temperature the measurements of the electrical impedance were conducted without an automatic temperature control in order to reduce electrical noise of the temperature controller. Each measured frequency scan of the complex resistance has been fitted to the expression as follows [19]

$$Z^* = \frac{R_1}{1 + (j\omega\tau_1)^{M_{HF}}} + \frac{R_2}{1 + (j\omega\tau_2)^{M_{LFD}}} \quad (1)$$

where the first and the second terms are responsible for high and low frequency dielectric losses, i.e. to two arcs on an Argand-type of diagram describing bulk and electrode polarization processes. In Eq. (1) parameters $0 < M_{HF}$, $M_{LFD} < 1$ are empirical constants characterizing a deviation of the observed dielectric loss peaks from a Debye-type function. Parameters τ_1, R_1, and M_{HF} are related to the bulk properties of sample or material properties measured at high frequency range (HF). The parameter M_{HF} in Eq. (1) describes a power law dispersion in a situation when the short range displacements of lattice defects become coupled with ionic environment. In ionic conductors with the increasing temperature M_{HF} may decreases from 1 to 0.5–0.6. The second term in Eq. (1) is called LFD [19]. The values of parameters R_2, τ_2 and M_{LFD} depends on the electrode polarization process, and, thus, traditionally have been omitted from the electrical impedance analysis. Nevertheless, during the structural phase transition, these parameters may vary significantly at the inversion point, because the quality and character of electrical contacts between polycrystalline sample and metal-electrodes depend on the crystal phase orientation or roughness of samples in contact with electrodes [20]. Because of this effective roughness the low frequency equivalent circuit may be represented as a infinite series of parallel capacitors and resistors with distributed RC-parameters (fractal model) according to a power law frequency dependence. When the sample material near the electrode experienced a phase transformation, the roughness of the sample-electrode interface changes and affects the low frequency signal. For dielectrics this change at low frequencies may be even more noticeable than the variation of bulk properties at high

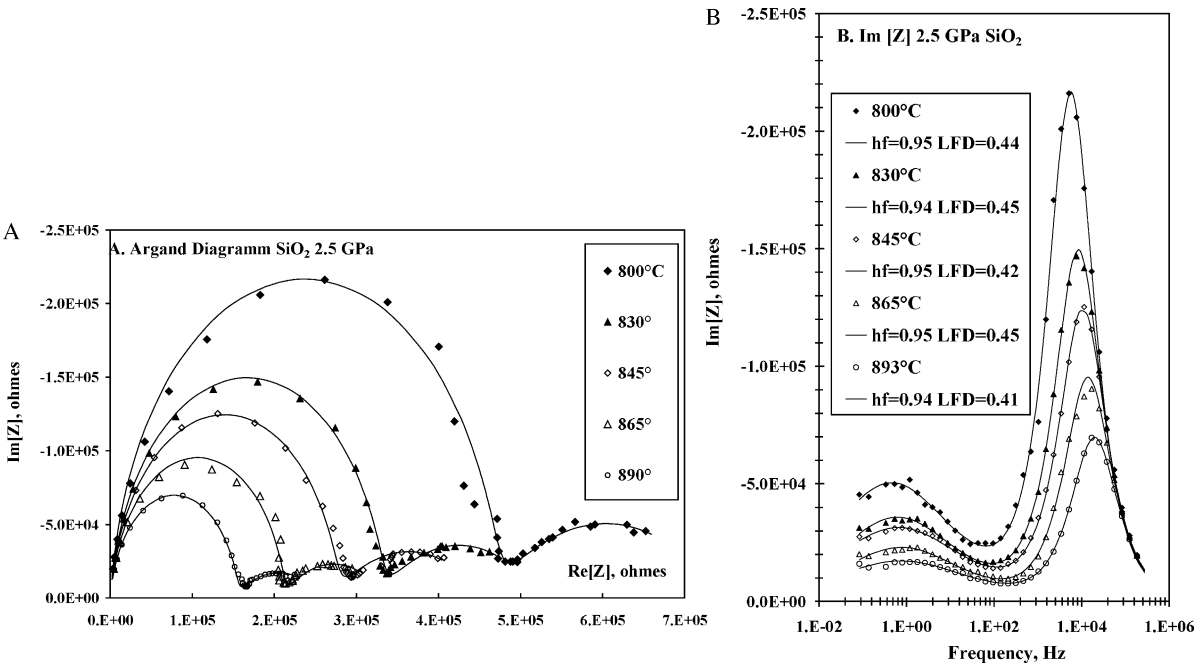

Fig. 1. Electrical impedance data measure for quartz at 2.5 GPa and presented (A) in the Argand diagram Im[Z] vs. Re[Z], and (B) in a plot imaginary component Im[Z] vs. frequency. The fitting parameters appeared in Eq. (1) are listed in Table 1.

Table 1
Fitting parameters of Eq. (1) for SiO_2 at 2.5 GPa

Temperature (°C)	R_{HF} (10^5 Ω)	R_{LFD} (10^5 Ω)	τ_{HF} (10^{-5} s)	τ_{LFD} (s)	M_{HF}	M_{LFD}
800	4.65	2.80	2.78	0.349	0.948	0.441
830	3.28	1.95	1.89	0.259	0.935	0.448
845	2.72	1.83	1.49	0.245	0.935	0.420
865	2.09	1.26	1.13	0.210	0.935	0.446
893	1.52	1.06	0.80	0.211	0.936	0.400

frequencies. The self-similarity of the length of grain boundaries may give rise to the power law frequency dependence of LFD measurements. The LFD contribution may be significant not only at insulator–metal interfaces, when the insulator possesses ionic conductivity, but also from space charge regions surrounding the grain boundaries [16].

The formation of concentration profiles or trapping layers of charge transporting ions on grain boundaries can also enhance the LFD contribution.

The bulk DC-conductivity of a sample is calculated from Eq. (1) according to $\sigma_{DC} = 1/R_1 G$, where G is a geometric factor of the measuring capacitor cell. In the case of a concentric cylinder capacitor $G = 2L/\ln(D/d)$, where L is the length, D and d are the outer and inner diameters of cylinder electrodes, respectively. The temperature dependence of the bulk conductivity follows an Arrhenian dependence as follows

$$\sigma_{DC} T = \sigma_0 \, e^{-(E_\sigma/kT)} \tag{2}$$

where T is in Kelvin, k is the Boltzmann's constant, σ_0 is the pre-exponential factor, E_σ is the activation energy of the electrical conductivity, characterizing an energetic barrier for the movement of charge carriers, i.e. lattice defects. Usually, in different temperature intervals the accuracy of the fitting parameters for the second term in the right-hand side of Eq. (1) varies significantly. For quartz samples the specific bulk conductivity is low, DC-dielectric relaxation time τ_1 is high and only 1–2 orders of magnitude lower than LFD relaxation time τ_2 in Eq. (1). These closeness of τ_1 and τ_2 permit to estimate with a good precision of all six parameters in Eq. (1) from a scan of electrical impedance in the frequency range 300 kH–30 mHz.

Electrical impedance scans were obtained at temperatures below and above the inversion temperate T_c during heating and cooling cycles and at stepwise increasing pressures from 0.5 to 2.5 GPa. The example of scan series obtained at 2.5 GPa and in the temperature range from 800 to 893 °C are shown in Fig. 1a and b. The fitting parameters are listed in Table 1. M_{HF} is varies insignificantly and close to 0.95, M_{LFD} is about 0.4–0.5. The shape of the high frequency data on the Argand-diagram is close to a perfect semi-circle left, which means that the left peak in Fig. 1a is almost of a Debye-type. This indicates on a single relaxation mechanism of the bulk electrical conductivity. The contributions of the bulk electrical conductivity which stems from twin boundaries seems to be insignificant, the shape of the high frequency semi-circle does not vary with the temperature. If the contribution of the twin boundary conductivity contributes significantly to the overall bulk conductivity, the resulted arc on the Argand diagram should be extended and the parameter $M_{HF} < 1$ in Eq. (1). Contrary to high frequency data, the low frequency data usually demonstrate much larger dispersion $M_{LFD} \ll 1$. M_{LFD} varies also with temperature, but this variation is continuous in the transformation temperature range.

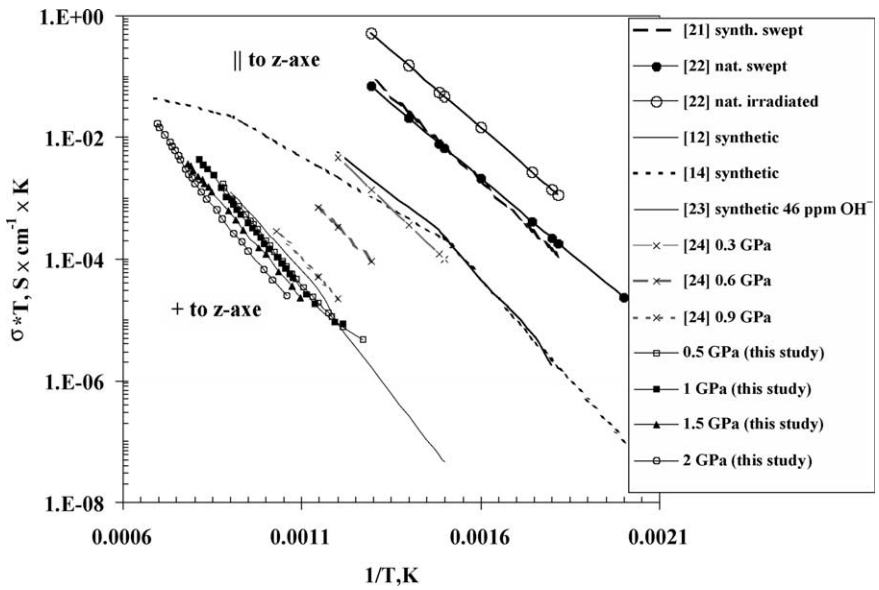

Fig. 2. Measurements of electrical conductivity in SiO_2 at atmospheric pressure (previous results in comparison with electrical impedance measurements at high pressure in this study). Measurements on single crystals parallel to the z-axis: swept synthetic sample [21], natural swept sample [22], synthetic non-swept samples [12,14,24], synthetic sample with 46 ppm of OH^- [23]. In this study polycrystalline compact powder samples were used.

3. Impedance measurements and α–β phase transition

3.1. Electrical conductivity

From R_1 of Eq. (1) estimated for each temperature and pressure, the bulk electrical conductivity has been calculated. The temperature–pressure dependence of the bulk DC-conductivity usually follows an Arrhenius-type of dependence

$$\sigma_1 T = \sigma_{0,1}\, e^{-(E_\sigma + P v_m/kT)} \quad (3)$$

where P is the pressure, v_m is the migration volume, E_σ is the activation energy of the electrical conductivity at normal pressure, k is the Boltzmann constant and $\sigma_{0,1}$ is the pre-exponential factor. The results are presented in Fig. 2. As it evidences from the plot, the pressure do not affect significantly σ_1, bulk electrical conductivity slightly decreases with pressure. In comparison with previous measurements, which have been done at atmospheric pressure on natural single crystals, synthetic doped crystals with Li ions [21] or swept crystals or synthetic samples oriented along z [14,24,25], the data of the electrical conductivity obtained in the present study are significantly lower than the reported data obtained on single crystals oriented along z-axis. Swept samples are samples submitted to a large electrical field 1 kV/cm for 1–2 days in order to remove alkaline ions from z-channels [22]. In the present study the polycrystalline samples were pressed from powder of natural SiO_2 and show isotropic electrical properties. Synthetic samples oriented along z-axis demonstrate also much higher conductivity [23]. At the same time measurements, which have been done on synthetic samples oriented perpendicular to the z-optical axis are close to the results of the present study [23]. The recent measurements of a phase in a single crystal at pressures 0.3–0.9 GPa [24] evidences also higher conductivity in comparison with the present study, measured on compacted polycrystalline samples. Thus, the difference between natural, synthetic and swept samples are smaller than the anisotropy of electrical conductivity in quartz. Pressure increase produces larger decrease of the electrical conductivity in the direction parallel to z-axis than in other directions. The data of the bulk and LFD electrical conductivities and dielectric relaxation times for pressure 0.5 GPa are shown in Fig. 3a and b. On the Arrhenius plot of $\sigma_1 T$ and $\sigma_2 T$ vs. $1/T$ the difference of activation energy in low temperature and high temperature phases can be

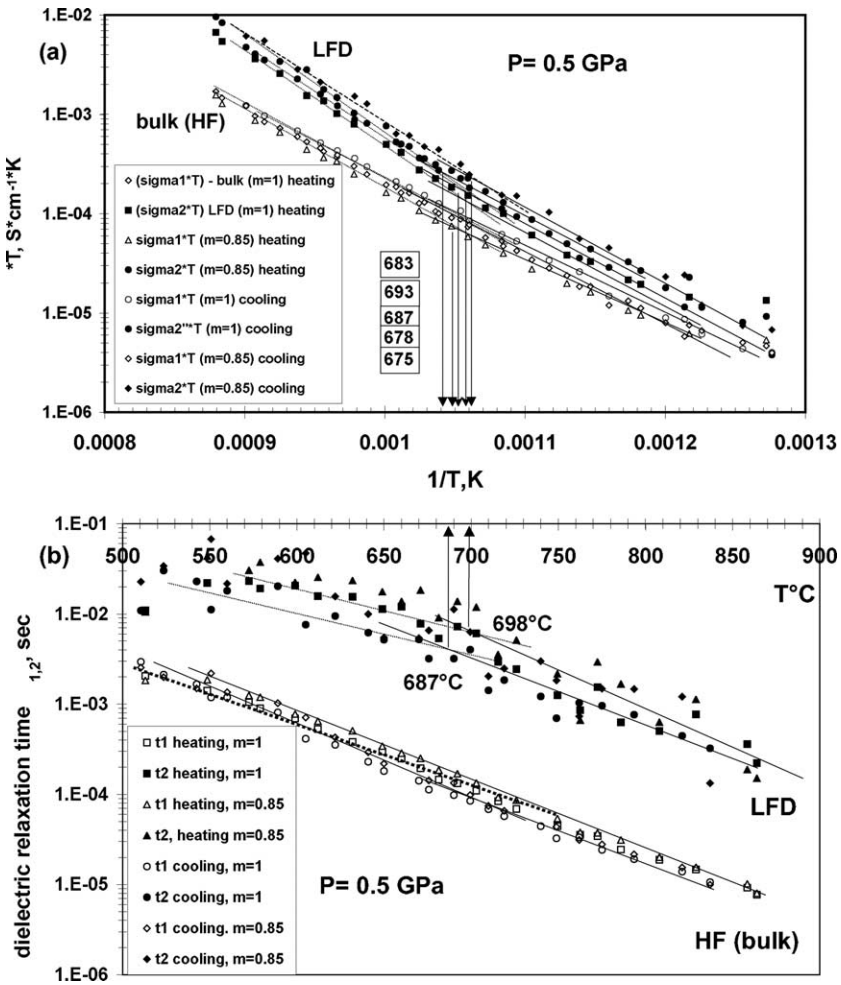

Fig. 3. $P = 0.5$ GPa. (a) Electrical conductivity and (b) dielectric relaxation time for bulk property measurements at HF and for LFD.

Table 2
Activation energy of E_s of the electric conductivity sT in SiO_2 (eV)

Pressure, GPa	$\alpha_{bulk\ HF}$	α_{LFD}	$\beta_{bulk\ HF}$	β_{LFD}
0.5	1.14	1.20	1.38	1.80
1	1.23	1.28	1.41	1.76
1.5	1.30	1.38	1.43	1.73
2	1.37	1.42	1.45	1.83
2.5	1.44	1.45	1.46	1.79

Note: Standard deviation of E_a measurements is ca. ± 0.04 eV.

appreciated from the slope of straight lines at $T > T_c$ and $T < T_c$. For $\sigma_1 T$ this difference is not appreciable. The calculated values of the activation energy are listed in Table 2. For the bulk electrical conductivity the difference between activation energies in two phases are within the experimental error. The kink point or T_c cannot be identified from these plots. For plots $\sigma_2 T$ vs. $1/T$ (upper lines in Fig. 3a) the kink point or the difference in the activation energy between two phases is much larger (see LFD data in Table 2). The same is true for dielectric relaxation time. The data for τ_1 seem to obey a straight line, contrary, the data of τ_2 indicate the kink point which corresponds to the inversion temperature point in quartz. The activation energy of bulk (HF) and LFD electrical conductivities below and above T_c correspond to the effective values of the activation energy of alkaline ion migration. E_σ depends on the association energy E_A of the alkaline ion to the aluminum and on the migration energy E_m : $E_\sigma = bE_A + E_m$ [26], where b is the empirical parameter ($0.5 < b < 1$) accounting the nature of the sample (~ 0.5 for natural samples, ~ 1 for synthetic samples). The difference in activation energy E_σ between natural, synthetic and irradiated samples can be explain as follows [22]. The ionic electrical conductivity is a product of a charge concentration and charge mobility. The charge mobility is an Arrhenius function of the temperature with an activation energy depending on an ion size and has a physical meaning of an energetical barrier for the elementary migration step. In irradiated samples alkaline ions or H^+ are mostly substituted by a hole h^+ (sweeping process). The calculated transition energy to an exited state of Al–h defect in quartz is 0.11 [27]. This is the lowest limit of the activation energy of electrical charge migration E_m in quartz. Calculated minimum potential surfaces for E_m along the z-axis provides 0.25 eV for Li^+, 0.27 for Na^+ and K^+ [28]. The experimental determination of mobility activation energy E_m of ionic impurities in quartz by means of electrical conductivity measurements at temperatures <273 K indicate the correctness of these calculations 0.26 eV [14]. The temperature dependence of charge carrier concentration depends on the association energy of the Al–M pair and the assumption whether these pairs are formed together (all Al–h defects are filled with alkaline ions or H^+) or the concentration of Al–h defects is much larger than concentration of alkaline ions (irradiated or synthetic samples). In the first case the concentration of charge carriers depends on temperature with an activation energy $= E_A/2$ and $b = 0.5$, in the second case the activation energy is twice larger $\sim E_A$ and $b \sim 1$ [22]. In radiation induced samples of α-quartz for Na^+ the activation energy of the electrical conductivity for Na^+ 0.76–1.38 eV, for $Li \sim 0.75$–1.25, and for $H^+ \sim 1.5$–1.9 eV [21,26]. The reported in Ref. [25] values of E_σ are 0.74–0.93 eV for Li^+, 0.91–1.09 for Na^+ and 1.21–1.38 for K^+. The listed in Table 2 values of activation energies of σT in α-phase are in a good agreement with the activation energies of alkalis in SiO_2. The activation energy of β-phase is larger and pressure independent. The migration volume of a charge carriers in β-phase is much smaller than in α-phase indicating the effect of H^+ as well on the electrical conductivity of quartz at high temperatures.

3.2. Inversion temperature

In order to estimate the inversion temperature of α–β transition in SiO_2 the frequency scans of the electrical impedance were proceeded by the use of Eq. (1) in two ways. In the first method M_{HF} and M_{LFD} were used as fitting parameters. M_{HF} varies between from 1 to 0.9 and M_{LFD} from 0.55 to 0.35. The calculated bulk (HF) and LFD electrical conductivities obtained by this method are indicated in Figs. 3 and 4 as σ_1 and σ_2. In the second method, M_{HF} and M_{LFD} were fixed and taken equal to the mean values 0.95 and 0.45, respectively. The difference in calculated conductivities and relaxation times by both the methods is within experimental error of the measurements. As it follows from Figs. 3 and 4, the bulk conductivity does not show any features at the inversion point of α–β quartz. The LFD conductivity clearly demonstrates the kink of the slope or a change in the activation energy $E_\sigma \cdot T_c$ estimated from the kink of the temperature dependence of LFD conductivity at pressures from 0.5 to 2.5 GPa is listed in Table 3. Previous studies of the temperature dependence of the electrical conductivity have been focused on the bulk property measurements at atmospheric pressure in single crystals. As a rule the inversion temperature have not been marked by any change of E_σ neither in natural nor in synthetic or irradiated samples measured parallel to the z-axis [22,23]. The decrease of the E_σ has been observed in synthetic samples at temperatures below T_c at 440 °C [14]. A small decrease of E_σ has been noticed in synthetic samples perpendicular to the z-axis with a decrease from 1.5 to 1.3 eV at 573 °C [23]. The activation energies in α and β phases at different pressures are listed in Table 4.

The slope of the inversion temperature from the results of LFD measurements is 233.51°/GPa (Fig. 5). This result compares well with the DTA method ~230°/GPa [29], but lower than other experimental estimations: 251°/GPa [30], 258°/GPa [31], 260°/GPa [32], and 255.9°/GPa [34]. The theoretically calculated slopes of the inversion temperature in quartz are poorly constrained: from experimental C_p data and the Birch–Murnaghan equation of state $dT_c/dP \sim 235.5$ [35]. From the change of volume at T_c estimated experimentally by measurements of lattice

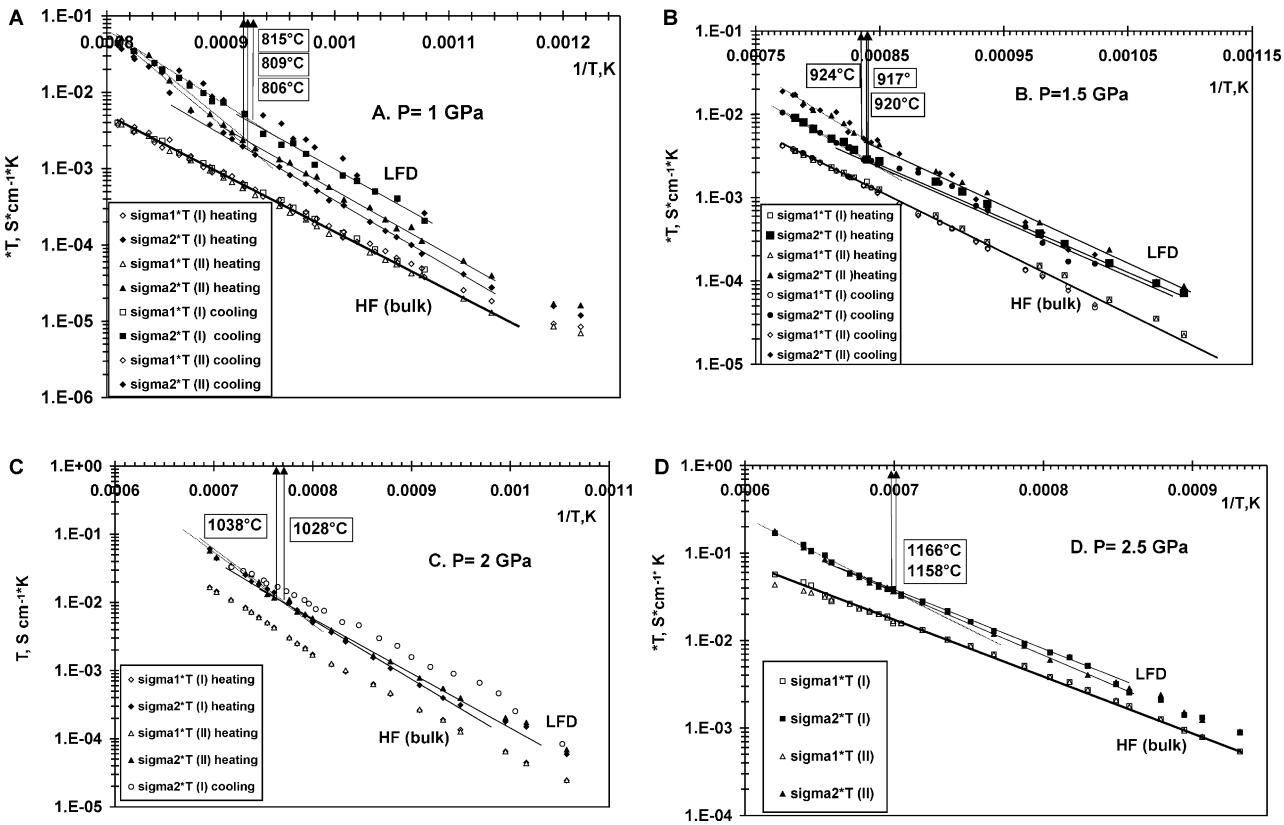

Fig. 4. Bulk (HF) and LFD conductivities of SiO_2 at pressures: (A) $P = 1$ GPa; (B) $P = 1.5$ GPa; (C) $P = 2$ GPa; (D) $P = 2.5$ GPa.

cell parameters $\sim 0.149\ \mathrm{cm}^{-1}$/mol and from Landau entropy at $T_c \sim 0.696$ J/mol [8], the slope must be 214 °C. Slightly better results can be obtained by the use of the quartz cell parameters of Ref. [37]: the spontaneous strain $= 2e_{11} + e_{33} = 6.43 \times 10^{-3}$. That provides a molar volume reduction $0.152\ \mathrm{cm}^{-1}$/mol and the slope ~218°/GPa. The reasonable slope 248°/GPa has been estimated in Ref. [36] considering the α–β transition as an order–disorder transformation, contrary to the fact of the high displaciveness of this transformation [9].

The calculated from Table 2 activation volume by the use of Eq. (3) is reported in Table 4. In the β-phase the activation energy of the bulk and LFD conductivities practically do not depend on pressure, the migration volume per particle $v_m \sim 0.02–0.06 \times 10^{-28}\ \mathrm{m}^{-1}$ (0.04 and 0.01 eV/GPa), in α-phase this dependence is appreciable v_m $0.21–0.24 \times 10^{-28}\ \mathrm{m}^{-1}$ (0.15 and 0.13 eV/GPa; Fig. 6). The activation volume measured on a single crystal parallel to the z-axis is $\sim 0.48 \times 10^{-28}\ \mathrm{m}^{-1}$ (0.3 eV/GPa) [24]. In the shock wave experiments, the estimated increase of the activation energy is $\sim 0.07 \times 10^{-28}\ \mathrm{m}^{-1}$ or ca. 0.04–0.05 eV/GPa [38]. Theoretical calculations of the pressure dependence of the fundamental band gap increase in the electronic structure of SiO_2 with the increasing pressure provide the migration volume $\sim 0.11 \times 10^{-28}\ \mathrm{m}^{-1}$

Table 3
T_c obtained from LFD electrical conductivity measurements

P, GPa	T_c, °C, α, β
0.5	683 ± 4
1.0	810 ± 4
1.5	920 ± 3
2.0	1032 ± 5
2.5	1162 ± 4

T_c determined as a kink point on the plot $\ln(\sigma T)$ vs. $1/T$ (K). The reported data are mean T_c values between cooling and heating cycles of two sequentially repeated runs.

Table 4
Activation energy and migration volume per particle of the electrical conductivity sT in SiO_2. (Fitting parameters of Eq. (3))

	E_σ, eV	V_m, $10^{-28}\ \mathrm{m}^{-1}$
Bulk HF, $T < T_c$	1.07	0.20
Bulk HF, $T > T_c$	1.37	0.06
LFD, $T < T_c$	1.15	0.18
LFD, $T > T_c$	1.76	0.02

Standard deviation of E_a estimation is ca. ±0.03 eV, v_m is ca. $\pm 0.02 \times 10^{-28}\ \mathrm{m}^{-1}$.

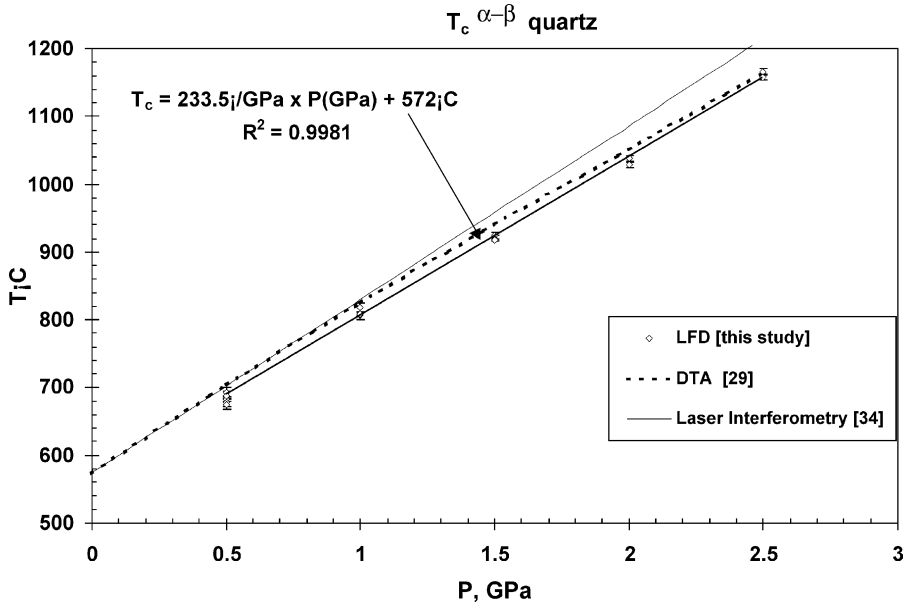

Fig. 5. T_c obtained from the kink of the temperature dependence of the LFD relaxation time. The obtain slope of the low-high quartz inversion temperature is 233.5°/GPa. The slope obtained experimentally and reported in the literature is (in °/GPa) 230 [29], 251 [30], 258 [31], 260 [32,33], 255.9 [34]. The calculated slope from C_p data and Birch–Murnaghan equation of state 235.5 [35], 248 [36], from the lattice cell parameters reduction and the Landau entropy 214 [8].

or ca. 0.07 eV/GPa [39]. The fact that in α-phase the migration volume is much larger than in β-phase supports the idea that in low temperature phase ionic concentrations and their mobilities are playing a major role on the overall conductivity of quartz, in β-phase at higher pressure these are, perhaps, only OH^- groups.

3.3. Dielectric relaxation time

The dielectric relaxation time τ_1 (bulk property) depends on temperature according to the Arrhenius equation

$$\tau_1 = \tau_{0,1}\, e^{(E_{ar}/kT)}, \tag{4}$$

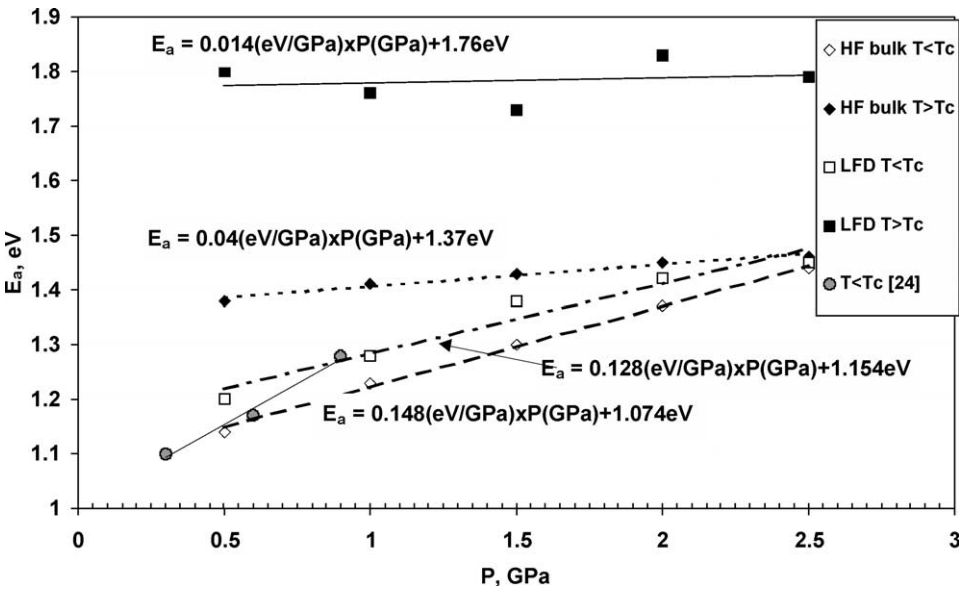

Fig. 6. Pressure dependence of the activation energy of the electric conductivity σT in quartz for HF (bulk) and LFD. The slope of linear dependence on pressure defines the migration volume v_m. For α-phase $v_m \sim (0.24 \pm 0.02) \times 10^{-28}$ m^{-1}, for β-phase $v_m \sim (0.06 \pm 0.02) \times 10^{-28}$ m^{-1}. The data from Ref. [24] for a single crystal α-phase parallel to the z-axis provide $v_m \sim 0.48 \times 10^{-28}$ m^{-1}.

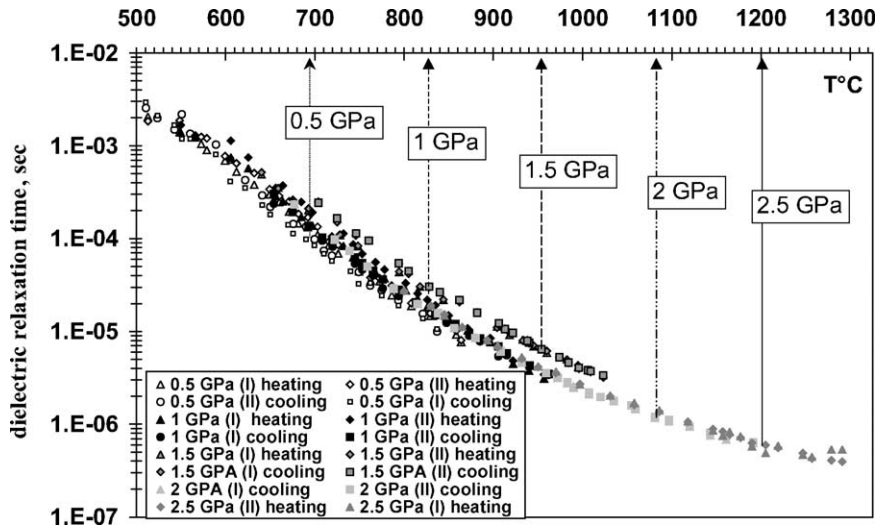

Fig. 7. Dielectric relaxation time for HF (bulk property) in quartz at pressures 0.5–2.5 GPa. The average fitting parameter of the Arrhenius dependence for τ are: $E_{a\tau} = 1.44 \pm 0.04$ eV, $\tau_0 = (5 \pm 2) \times 10^{-12}$ s.

where $E_{a\tau}$ is the activation energy of the dielectric relaxation time and $\tau_{0,1}$ is the pre-exponential factor. The results of measurements of τ_1 for pressures from 0.5 to 2.5 GPa are presented in Fig. 7 as a function of T in °C. The graph demonstrates that the pressure does not change the bulk dielectric relaxation time, all data are located on the same master curve. If the conductivity of quartz was purely ionic due to the alkaline ions, the dielectric relaxation time should have much stronger pressure dependence. The fitting parameter of this single curve are $E_{a\tau} \sim 1.44$ eV, $\tau_{0,1} \sim 5 \times 10^{-12}$ s. The low temperature ($T < 200$ K) dielectric relaxation in quartz crystal is 0.13–0.25 eV [40]. The main contribution to the dielectric relaxation at these temperatures is purely migration of Al^{3+}–h^{+} and Al^{3+}—alkaline ion pairs. The calculated values of $E_{a\tau}$ at constant pressure in α and β phases are listed in Table 5. These values are about 1.4–1.5 eV. The contribution from association reaction plus mobility from Al^{3+}–H^{+} and Al^{3+}–alkaline ion pairs is at these temperatures obvious. The difference between the activation energy of the bulk dielectric relaxation time in α and β phases of SiO_2 is about the experimental error of their determinations ca. 0.05 eV.

4. Conclusions

1. The determination of the inversion temperature in quartz by means of the electrical conductivity measurements is possible, if one includes into analysis the LFD data. The observed contrast of the activation energies between α and β phases for the LFD conductivity provides a reliable indication of the inversion temperature. The results of this study demonstrated workability of this method, and the experimentally determined slope of dT_c/dP in the range of 0.5–2.5 GPa is ~233.5°/GPa. The method can be applied to other compounds having a quartz-like structure and possessing the α–β transformation, for example, berlinite $AlPO_4$ and $FePO_4$.
2. The conductivity data and calculated activation energies in quartz samples pressed from powder of a natural single crystal are close to the results obtained on synthetic single crystals oriented perpendicular to the z-axis [23]. In natural quartz rocks without preferable orientation of quartz crystals will possess lower electrical conductivity in comparison with the z-axis values. Thus, small anisotropy of quartz rocks may be expected.
3. Pressure plays a minor role on the electrical conductivity and dielectric relaxation time of the polycrystalline quartz samples. The activation volume of the electrical conductivity in α-phase is several times larger than in β phase indicating that in two phases differing proportion of ion types (alkalis and H^{+}) may be responsible for the overall electric charge transport.

Table 5
Activation energy and preexponential factor of the dielectric relaxation time for α and β phases of SiO_2 (fitting parameters of Eq. (4))

P, GPa	$E_{a\tau}$, eV ($T < T_c$)	$E_{a\tau}$, eV ($T > T_c$)	τ_0, s ($T < T_c$)	τ_0, s ($T > T_c$)
0.5	1.44	1.41	2×10^{-11}	4.5×10^{-12}
1	1.58	1.55	7×10^{-12}	1.6×10^{-12}
1.5	1.55	1.51	1×10^{-11}	2.8×10^{-11}
2	1.53	1.48	3×10^{-12}	5×10^{-12}
2.5	1.41	1.37	7×10^{-12}	1.3×10^{-12}

Standard deviation of E_a is ca. ±0.04 eV.

Acknowledgements

The authors are grateful to J. Maumus (IfMG, Frankfurt) for the help with the piston-cylinder experiments, F. Brunet (ENS, Paris) for the sample of the natural quartz Monte Rose and the anonymous reviewer for the suggestions to improve the manuscript.

References

[1] G. Dolino, The α-inc-β transitions of quartz: a century of research on displacive phase transitions, Phase Transitions 21 (1990) 59–72.
[2] P.J. Heaney, in: P.J. Heanley, C.T. Prewitt, G.V. Gibbs (Eds.), Reviews in Mineralogy 29, Mineralogical Society of America, Washington, 1994, pp. 1–40.
[3] E. Philippot, D. Palmier, M. Pintard, A. Groiffon, A general survey of quartz and quartz-like materials: packing distortions, temperature, and pressure effects, J. Solid State Chem. 123 (1996) 1–13.
[4] J.F. Scott, Evidence of coupling between one- and two-phonon excitations in quartz, Phys. Rev. Lett. 21 (1968) 907–910.
[5] F. Gervais, B. Piriou, Temperature dependence of transverse and longitudinal optic modes in the alpha and beta phases of quartz, Phys. Rev. B 11 (1975) 3944–3950.
[6] J.P. Bachheimer, G. Dolino, Measurements of the order parameter of α-quartz by a second-harmonic generation of light, Phys. Rev. B (1975) 113195–113205.
[7] G. Dolino, P. Bastie, The role of incommensurate phase in the opalescence of quartz, J. Phys.: Condens. Matter 13 (2001) 11485–11501.
[8] M.A. Carpenter, E.K.H. Salje, A. Graemer-Barber, B. Wruck, M.T. Dove, K.S. Knight, Calibration of excess thermodynamic properties and elastic constant variations associated with α β phase transition in quartz, Am. Mineral. 83 (1998) 2–22.
[9] M.T. Dove, M. Gambhir, V. Heine, Anatomy of a structural phase transition: theoretical analysis of the displacive phase transition in quartz and other silicates, Phys. Chem. Miner. 26 (1999) 344–353.
[10] H. Schober, D. Strauch, K. Nützel, B. Domer, Lattice dynamics of α-quartz. II. Theory, J. Phys.: Condens. Matter 5 (1993) 6155–6164.
[11] C.M. Carbonaro, V. Fiorentini, S. Massidda, Ab-initio study of oxygen vacancies in α-quartz, J. non-Cryst. Solids 221 (1997) 89–96.
[12] P. Campone, M. Magliocco, G. Spinolo, A. Vedda, Ionic transport in crystalline SiO_2: the role of alkali–metal ions and hydrogen impurities, Phys. Rev. B 52 (1995) 15903–15908.
[13] J. Toulouse, S. Ling, A.S. Nowick, Dielectric relaxation of the aluminium-hole center in α-quartz: an example of phonon-assisted tunneling, Phys. Rev. B 37 (1988) 7070–7078.
[14] M. Martini, A. Paleari, G. Spinolo, A. Vedda, New high-temperature results on the ionic conductivity of quartz and implications on the transport mechanism, J. Appl. Phys.: Condens. Matter 2 (1990) 6921–6927.
[15] M. Calleja, M.T. Dove, E.K.J. Salje, Anosotropic ionic transport in quartz: the effect of twin boundaries, J. Phys.: Condens Matter 13 (2001) 9445–9454.
[16] J. Maier, On the conductivity of polycrystalline materials, Ber. Bunsenges. Phys. Chem. 90 (1986) 26–33.
[17] J.C. Brice, Crystals for quartz resonators, Rev. Mod. Phys. 57 (1985) 105–146.
[18] N. Bagdassarov, N. C, H. Freiheit, A. Putnis, Electrical conductivity and pressure dependence of trigonal-to-cubic phase transition in lithium sodium sulphate, Solid State Ion. 143 (2001) 285–296.
[19] A.K. Jonscher, Low-loss dielectrics, J. Mater. Sci. 34 (1999) 3071–3082.
[20] S.H. Liu, Fractal model for the ac response of a rough interface, Phys. Rev. Lett. 55 (1985) 529–532.
[21] C. Poignon, G. Jeandel, G. Morlot, Study of ionic impurity in quartz crystals by impedance and thermoionic current measurements, J. Appl. Phys. 80 (1996) 6192–6197.
[22] H. Jain, A.S. Nowick, Electrical conductivity of synthetic and natural quartz crystals, J. Appl. Phys. 53 (1982) 477–484.
[23] J.C. Newton-Howes, A.C. McLaren, R.J. Fleming, An investigation of the effects of hydroxyl concentration and bubble formation on the electrical conductivity of synthetic quartz, Tectonophysics 158 (1989) 335–342.
[24] D.-J. Wang, H.-P. Li, C.-Q. Liu, L. Yi, D.-Y. Ding, G.-L. Su, W.-G. Zhang, Electrical conductivity of synthetic quartz crystals at high temperature and pressure from complex impedance measurements, Chin. Phys. Lett. 19 (2002) 1211–1213.
[25] A.K. Kronenberg, S.H. Kirby, Ionic conductivity of quartz: DC time dependence and transition of charge carriers, Am. Miner. 72 (1987) 739–747.
[26] J. Plata, J. Breton, Theoretical model for the electrodiffusion of M^+ (M = Li, Na, K) ions in a quartz crystal, Phys. Rev. B 38 (1988) 3482–3493.
[27] M. Magagnini, P. Gianozzo, A. Dal Corso, Microscopic structure of the substitutional Al defect in α quartz, Phys. Rev. B 61 (2000) 2621–2625.
[28] J. Breton, J.C. Girardet, Al–M^+ centers (M = Li, Na, K) in a quartz crystal: potential surfaces, Phys. Rev. B 33 (1986) 8748–8754.
[29] P.W. Mirwald, H.-J. Massone, The low-high quartz and quartz-coesite transition to 40 kbar between 600 °C and 1600 °C and some reconnaissance data on the effect of $NaAlO_2$ component on the low quartz-coesite transition, J. Geophys. Res. 85 (1980) 6983–6990.
[30] A.F. Koster van Groos, J.P. ter Heege, The high-low quartz transition up to 10 kilobars pressure, J. Geol. 81 (1973) 717–724.
[31] R.S. Coe, M.S. Paterson, The α–β inversion in quartz: a coherent phase transition under nonhydrostatic stress, J. Geophys. Res. 74 (1969) 4921–4948.
[32] L.H. Cohen, W. Klement Jr., High-low quartz inversion: determination to 35 kbar, J. Geophys. Res. 72 (1967) 4245–4251.
[33] L.H. Cohen, W. Klement Jr., H.G. Adams, Yet more observations on the low quartz inversion: thermal analysis studies to 7 kbar with single crystal, Am. Mineral. 59 (1974) 1099–1104.
[34] A.H. Shen, W.A. Bassett, I.-M. Chou, The α–β quartz transition at high temperatures and pressures in a diamond-anvil cell laser interferometry, Am. Mineral. 78 (1993) 694–698.
[35] P.I. Dorogokupets, Equation of state for lambda transition in quartz, J. Geophys. Res. 100 (1995) 8489–8499.
[36] T.V. Gerya, K.K. Podlesskii, L.L. Perchuck, V. Swamy, N.A. Kosyakov, Equation of state of minerals for thermodynamic databases used in petrology, Petrology 6 (1998) 511–526.
[37] K. Kihara, An X-ray study of the temperature dependence of the quartz structure, Eur. J. Mineral. 2 (1990) 2–77.
[38] K.-I. Kondo, A. Sawaoka, Electrical measurements on fused quartz under shock compression, J. Appl. Phys. 52 (1981) 5084–5089.
[39] N. Binggelli, N. Troullier, J.L. Martins, J.R. Chelikowsky, Electronic properties of α-quartz under pressure, Phys. Rev. B 44 (1991) 4771–4777.
[40] D.S. Park, A.S. Nowick, Dielectric relaxation of point defects in α-quartz, Phys. Status Sol. (a) 26 (1974) 617–626.